Force Tracking Control for Lower Limb Exoskeleton Robot based on Chaos Light Spectrum Optimizer

Lie Yu, Zhuo Wu, Cong Zhang and Lei Ding

Abstract—**Exoskeleton robots can effectively enhance human motor performance, aid in rehabilitation and therapy, and provide greater comfort, safety, and efficiency for individuals. Most exoskeleton robots use hydraulic actuators, so the response speed and accuracy of the hydraulic cylinder directly affect the robot's performance. In this study, the kinematics and statics of the hydraulic cylinder are investigated, and a structural model is developed. In order to improve the control accuracy of the hydraulic cylinder, this study proposes a novel chaos mapping based light spectral optimization (CLSO) algorithm for designing proportional integral differential (PID) controllers for optimal force regulation of the hydraulic cylinder. In order to verify the effectiveness of the control method, an experimental study was conducted using the built-in model in Matlab. The experimental results show that the step response time of the CLSO-PID controller is reduced by 22% compared to the standalone LSO-PID maker. The delay time of the sinusoidal signal is reduced by about 33.3% and the error of the square wave signal is reduced by 12.48%. The results show that the control performance is significantly improved by the CLSO-PID controller.**

Index Terms—**PID, Hydraulic cylinders, Exoskeleton robot, LSO, Chaos.**

I. Introduction

EXOSKELETON robots are utilized across various domains including rehabilitation training, medical treatment, and military applications. It is an integrated electromechanical device that can be worn externally on the human body, aimed at enhancing, assisting, or restoring human motor abilities and functions. Due to its ability to provide high-power density [1], smooth and precise motion control, suitability for high-power applications, and excellent adjustability allowing for pressure and flow rate adjustments to meet various application requirements [2], hydraulic systems are commonly employed in the design and construction of exoskeleton robots [3]. Typically, the control systems listed are basic, sluggish, and lack precise sensors and feedback control loops [4]-[5]. The performance and effectiveness of exoskeleton systems heavily rely on the level of control algorithm sophistication and intelligence [6]. Further research and development of advanced control methods and human-machine interaction technologies is essential to enhance the flexibility and adaptability of the system [7]-[8].

Numerous studies have investigated the application of advanced controllers, such as neuro fuzzy controllers, sliding mode controllers, and fractional order PID controllers, for controlling hydraulic systems, often with good results [9]. However, even with minor changes in system parameters, the proposed controllers may still lead to instability and loss of control [10]. Typically, this occurs because these controllers are designed for specific systems, with parameter adjustments and performance optimization based on system characteristics and dynamic models. Therefore, even minor parameter variations may exceed the controllers' design scope, resulting in degraded system performance or even collapse. Addressing this issue requires the adoption of more robust and adaptive control strategies to enable the system to better accommodate parameter changes and external disturbances, thereby enhancing system stability and robustness.

The movement of the robotic arm has significant nonlinear characteristics and its torque due to gravity varies nonlinearly with the pitch angle, resulting in the hydraulic cylinder motion model becoming a complex system containing nonlinear uncertainties. Consequently, achieving precise positioning in hydraulic servo systems necessitates highly accurate mathematical models. The development of such models, however, encounters significant obstacles due to inherent system complexities. Contributing factors include flow dead zones, stiction phenomena within the fluid media, fluid compressibility coupled with internal leakage, and the non-proportional relationship between flow rate and pressure inherent in control valves. These combined effects result in complex nonlinear dynamics with substantial parametric uncertainties.Recent research has intensified focus on hydraulic servo system modeling [11]. Mete et al. [12] established a nonlinear mathematical framework addressing electro-hydraulic servo dynamics, incorporating component-level interactions under internal leakage effects. Their investigation quantified leakage-induced positional control degradation. Concurrently, Yao et al. [13] developed an adaptive inverse model leveraging system parameter awareness, implementing real-time nonlinearity compensation through recursive estimation. These breakthroughs establish robust methodologies for resolving hydraulic system nonlinearities.

Proportional-Integral-Derivative (PID) control remains ubiquitous across industrial applications since its inception

Manuscript received December 9, 2024; revised July 1, 2025.

This work was supported by the National Natural Science Foundation of China "Research on motion pattern recognition of exoskeleton robot based on curve similarity model" (NO.62106178).

Lie Yu is an associate professor of School of Electronic and Electrical Engineering, Wuhan Textile University, Wuhan, China. (corresponding author to provide phone: +86 18607155647; e-mail: lyu@wtu.edu.cn).

Zhuo Wu is a postgraduate student of School of Electronic and Electrical Engineering, Wuhan Textile University, Wuhan, China. (e-mail: 16602754984@163.com)

Cong Zhang is a postgraduate student of the School of Electronic and Electrical Engineering, Wuhan Textile University, Wuhan, China. (e-mail: zc_yyds@163.com)

Lei Ding is an associate professor at School of Computer Science and Artificial Intelligence, Wuhan Textile University, Wuhan, China. (e-mail: lding@wtu.edu.cn)

[14]-[15]. Recent methodological advances include: Wang's internal model control (IMC)-based PID parameterization for integrator/dead-time processes, albeit limited in disturbance rejection [16]. Normey-Rico's unified tuning framework accommodating stable/integral/unstable dynamics with dead-time, achieving simultaneous robustness enhancement and disturbance attenuation [17]. Despite its widespread application across various industrial processes, traditional PID control often exhibits unsatisfactory performance, particularly in non-linear systems. This inadequacy stems from the presence of unknown and nonlinear effects, which can compromise the control's effectiveness. The AI-driven paradigm shift has catalyzed novel computational frameworks for PID controller enhancement. Core methodologies encompass neural networks, fuzzy systems, evolutionary computation, and stochastic optimization, demonstrating significant implementation efficacy in control systems. Exemplary cases include: Bassi's stochastic parameter optimization via particle swarms in linear motor PID tuning [18]. Chiou's PSO-synthesized fuzzy-PID controller suppressing nonlinear dynamics in active suspensions [19]. Zadeh L. A. [20] put forward Fuzzy logic control can handle fuzzy and uncertain information and adaptively adjust the controller output based on fuzzy rules to better meet the control requirements of complex systems. Building upon computational intelligence frameworks, Lei Liu harnessed Radial Basis Function (RBF) networks to characterize unmodeled dynamic uncertainties in nonlinear switching systems. Notwithstanding this advancement, persistent steady-state offsets manifested in system outputs [21]. Concurrently, Wang Y pioneered a hybrid PID architecture synergistically merging fuzzy-PID adaptability with predictive function control's anticipatory capabilities [22]. In [20] introduces a self-optimizing neural control architecture featuring progressively constructed radial basis function networks (GRBFNs) to address nonlinear flight dynamics. In [23], a self-tuning PID control framework was developed that integrates cellular genetic algorithms for improved adaptive performance. [24]employed radial basis function neural networks to establish predictive correlations between interior climate parameters (temperature and humidity) and external environmental drivers (ambient temperature and solar irradiance) within hydroponic greenhouse environments [25]-[26]. Evolutionary and stochastic optimization techniques—including genetic algorithms and simulated annealing—facilitate parametric exploration within high-dimensional solution spaces. This enables precision calibration of PID controllers for enhanced dynamic response and stability margins [27]-[28]. Hence, the introduction of intelligent algorithms provides new pathways and possibilities for improving PID controllers, driving the development and progress of the control field. This study develops a spectral optimization framework employing enhanced chaotic mapping to tune PID parameters. The Chaotic Light Spectrum Optimizer (CLSO) significantly attenuates steady-state error in hydraulic servo positioning, accelerates system response, and suppresses external disturbance propagation. Comprehensive evaluations demonstrate CLSO-PID's capacity for near-perfect reference tracking.

II. System Modeling

This section derives a dynamic model of the hydraulic-actuated mechanical leg, emphasizing nonlinear hydraulic cylinder dynamics and actuator-leg force transmission. The modeling methodology leverages established nonlinear formulations for hydraulic actuators [29,30], with the physical system configuration and mathematical representation detailed in Fig. 1.

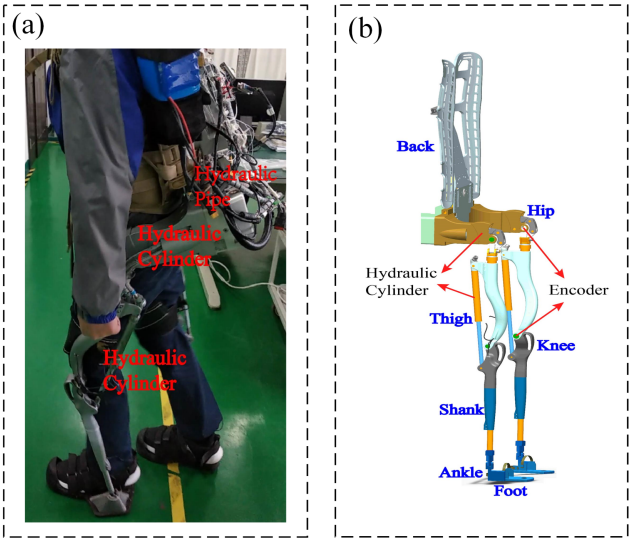

Fig. 1: Material object and modeling of the machine leg.

The hydraulic cylinder diagram is shown in Fig. 2 , driving force equations are as follows:

g	Acceleration due to gravity
A_{p1}	Head-side area
A_{p2}	Rod-side area
D_1	Bore diameter
D_2	Rod diameter
V_1	Rodless side cylinder volume
V_2	Rod side cylinder volume
k_q	Valve discharge gain
β	Effective bulk modulus
C_t	Coefficient of the total internal leakage
P_r	Oil return pressure
P_s	Oil supply pressure
P_1	Rod-side pressure
P_2	Rodless-side pressure
Q_1	Inlet chamber flow rate
Q_2	Outlet chamber flow rate
X_p	Hydraulic cylinder displacement
X_v	Spool position
F_L	Driving force

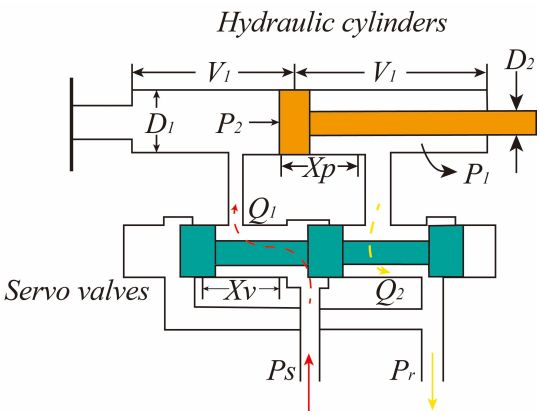

Fig. 2: Hydraulic cylinder model.

$$\begin{cases} \dot{F}_L = A_{p1}\left[\left(\dfrac{R_1}{V_1}+\dfrac{R_2}{V_2}\right)\beta k_q x_\nu \right. \\ \qquad \left. -\left(\dfrac{1}{V_1}+\dfrac{1}{V_2}\right)\left(\beta C_t\left(P_1-P_2\right)\right)\right] \\ \dot{P}_1 = \dfrac{\beta}{V_1}\left(-C_t P_1 + Q_1\right) \\ \dot{P}_2 = \dfrac{\beta}{V_2}\left(C_t P_1 - Q_2\right) \end{cases} \tag{1}$$

where P_L=P_1-P_2 is the load pressure of the dynamic actuator. Q_1 and Q_2 denote the flow rates in the chambers, which can be calculated using the following equations:

$$\begin{cases} Q_1 = k_q x_v[s\left(x_v\right)\sqrt{P_s - P_1} + s\left(-x_v\right)\sqrt{P_1 - P_r}] \\ Q_2 = k_q x_v[s\left(x_v\right)\sqrt{P_2 - P_r} + s\left(-x_v\right)\sqrt{P_s - P_2}] \end{cases} \tag{2}$$

Q_1 and Q_2 are both related to spool valves (x_v). The s(x_v) can be described as:

$$s\left(x_v\right) = \begin{cases} 1, & x_v \geq 0, \\ 0, & x_v \leq 0, \end{cases} \tag{3}$$

Under practical operation, P_1 and P_2 are subject to the constraints:

$$0 < P_r < \min(P_1, P_2) \quad \text{and} \quad P_2 < P_s \tag{4}$$

where P_s denotes the saturation pressure and P_r the reference pressure.

III. Controller Design

A. Design of PID controller

In traditional industries, the application of PID controllers is mature, with advantages such as simple principles, strong robustness, and wide practicality. It is a mature technology and the most widely used control system, as shown in Fig. 3.

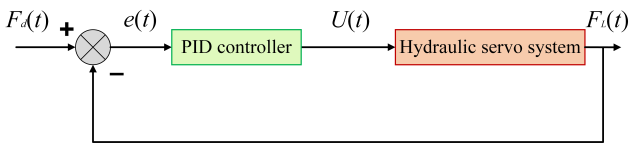

Fig. 3: Hydraulic servo system PID control.

The control structure of the system's PID controller is as follows:

$$i\left(t\right) = K_p e\left(t\right) + K_i \int e\left(t\right) dt + K_d \frac{de\left(t\right)}{dt} \tag{5}$$

where *e(t)* = $F_d(t)$ - *F(t)*represents the error between the desired position and the actual position of the hydraulic cylinder.

B. Design of CLSO-PID controller

Precision calibration of proportional-integral-derivative (PID) parameters remains an enduring design dilemma in control systems. While metaheuristic techniques—notably particle swarm optimization (PSO), simulated annealing (SA), and genetic algorithms (GA)—have demonstrated efficacy in parameter tuning, this research introduces a chaotic light spectrum optimizer (CLSO) framework. The CLSO algorithm emulates adaptive spectral dispersion and extremum-seeking behaviors fundamental to dispersive light-matter interactions.

Specifically, the algorithm is derived from Descartes' law of refraction, where white light disperses into seven chromatic components (red, orange, yellow, green, blue, indigo, violet) when transitioning between media with distinct refractive indices. By mathematically simulating this spectral dispersion process, the CLSO dynamically adjusts two key parameters: 1) the resolution of the PID parameter search space, and 2) the convergence velocity. This dual-adaptive mechanism enables rapid and precise identification of optimal PID gains for servo-electric cylinder control in lower-limb exoskeletons. Notwithstanding its computational intensity, the light spectrum optimizer (LSO) exhibits superior convergence rate compared to conventional metaheuristic counterparts. Nevertheless, two inherent constraints hinder its practical implementation in exoskeleton control systems: (1) the stochastic nature of its exploration patterns, and (2) suboptimal balance between global exploration and local exploitation due to parameter space resolution and search velocity constraints.

To address these limitations, we propose a chaotic-enhanced LSO (CLSO) algorithm through integration of chaotic mapping operators. This modification leverages the ergodic properties of chaotic systems to systematically regulate the search trajectory, thereby achieving dynamic equilibrium between wide-range exploration and localized refinement. The implemented chaotic mechanism ensures non-repetitive traversal of the PID parameter space while maintaining deterministic optimization paths – a critical feature for real-time servo control applications. The detailed computational workflow is illustrated in Fig. 4, demonstrating the synergistic integration of spectral analysis principles with chaotic dynamics.

1) Initialization Step : The Light Spectrum Optimizer (LSO) initiates its search process through stochastic initialization of the white light ensemble:

$$\overrightarrow{x_1} = lb + Rv_1(ub - lb) \tag{6}$$

where $R_{v1} \in R^{dim}$ denotes a uniformly distributed random vector on $[0, 1]$, with dimensionality dim corresponding to the PID control parameters (K_p, K_i, K_d). The solution

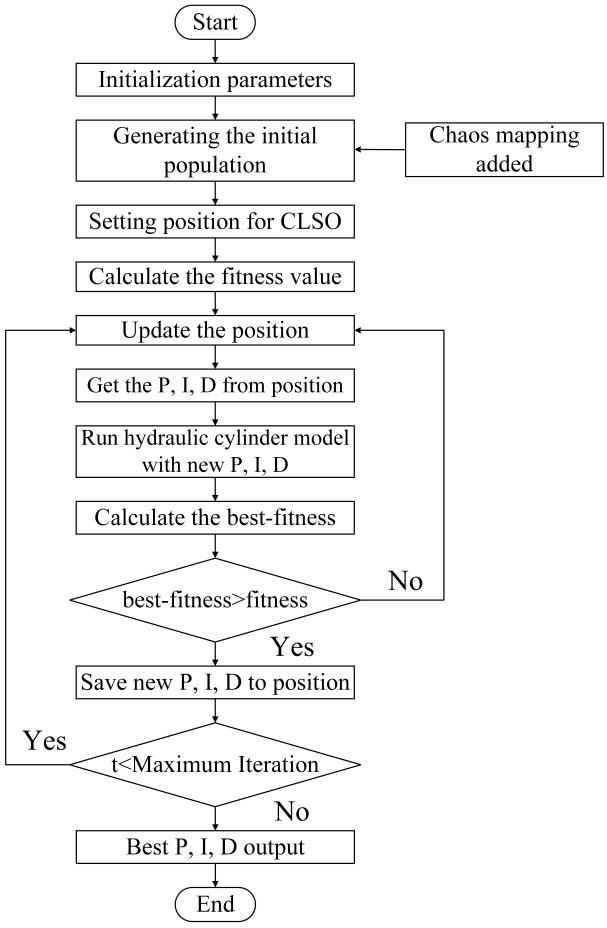

Fig. 4: CLSO flowchart.

space boundaries are defined by *lb* (lower bound) and *ub* (upper bound). These initial solutions undergo fitness evaluation to establish both personal and global optima.

2) Chaos Map : The generation of individuals in the initial population of most population intelligence algorithms is randomized within a given range, resulting in significant randomness and uncertainty in the initial individuals. However, the addition of chaotic mapping can greatly increase the randomness of the initial individuals.

Chaotic systems characterize non-linear deterministic dynamics that exhibit extreme sensitivity to initial conditions, aperiodic behavior, and inherent stochasticity. These systems are broadly classified into two categories: low-dimensional chaos (LDC) and high-dimensional chaos (HDC). While HDC systems possess intricate topological structures and enhanced parameter control capabilities, their practical implementation in real-time control systems is constrained by prohibitive computational demands. Conversely, LDC systems offer implementation simplicity through reduced parametric dimensionality, yet suffer from three critical limitations: (1) restricted chaotic attractor diversity, (2) discontinuous phase-space topologies, and (3) distributional non-uniformity in output sequences.

To overcome these inherent constraints, we propose a hybrid chaotic mapping architecture through synergistic integration of elementary LDC components. The developed Sine-Tent-Cosine (STC) composite mapping exemplifies this paradigm, formulated as:

$$x\left(i+1\right)=\begin{cases} if \quad x(i)<0.5 \\ cos\big(\pi\big(r\sin\left(\pi x(i)\right) \\ +2(1-r)x(i)-0.5\big)\big) \\ else \\ cos\big(\pi\big(r\sin\left(\pi x(i)\right) \\ +2(1-r)\big(1-x(i)\big)-0.5\big)\big) \end{cases} \tag{7}$$

$$r\in[0,1] \tag{8}$$

This enhanced chaotic framework effectively mitigates intrinsic limitations of low-dimensional chaotic systems while maintaining higher computational tractability than high-dimensional alternatives. The resultant implementation efficiency is validated through chaotic initialization profiles depicted in Fig. 5 and Fig. 6.

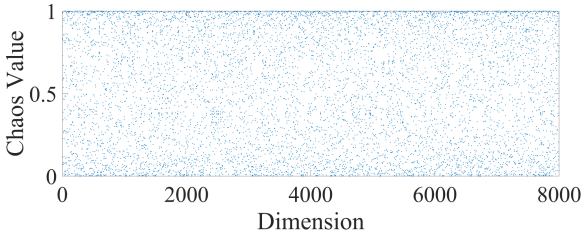

Fig. 5: Points generated randomly by chaotic mapping

3) Colorful Dispersion of Light Rays : Following initialization, the internal refraction normal vector, internal reflection normal vector, and external refraction normal vector are calculated as follows. The normal vector of inner refraction $\vec{x_{nA}}$, inner reflection $\vec{x_{nB}}$, and outer refraction $\vec{x_{nC}}$ are calculated as:

$$\vec{x_{nA}}=\frac{\vec{x_t^r}}{norm\left(\vec{x_t^r}\right)} \tag{9}$$

$$\vec{x_{nB}}=\frac{\vec{x_t^p}}{norm\left(\vec{x_t}\right)} \tag{10}$$

$$\vec{x_{nC}}=\frac{\vec{x_t^r}}{norm\left(\vec{x^*}\right)} \tag{11}$$

where $\vec{x_t^r}$ denotes a stochastically selected population member at iteration t, $\vec{x_t^p}$ represents the incumbent solution at t, $\vec{x^*}$ signifies the historical global optimum. The normalization operator norm(.) transforms vectors according to:

$$norm\left(\vec{x}\right)=\sqrt{\sum_{j=0}^{d}x_j^2} \tag{12}$$

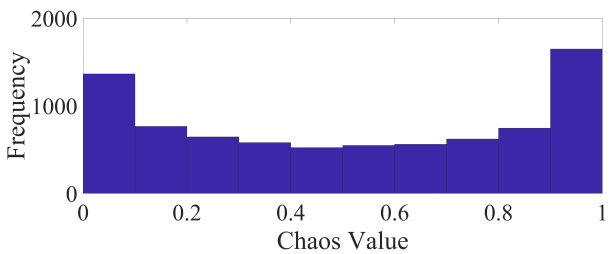

Fig. 6: Chaos mapping distribution rate (0-1).

where $d \in Z^+$ denotes the problem dimensionality, $\vec{x}$ represents the input vector for normalization, and x_j corresponds to the j^{th} component of $\vec{x}$. The incident light ray vector is computed as:

$$X_{mean} = \frac{\Sigma_{\text{i}}^{\text{N}} \vec{x}_i}{N} \tag{13}$$

$$\vec{x_{L0}} = \frac{x_{mean}}{norm\,(x_{mean})} \tag{14}$$

where x_{L0} denotes the incident light intensity, $\overline{\mathbf{X}} = \frac{1}{N}\sum_{i=1}^{N} \mathbf{x}_i$ represents the population mean of current solutions, and N is the population size. The refraction and reflection vectors are subsequently computed for both internal and external interfaces:

$$\begin{aligned} \vec{x_{L1}} = &\frac{1}{k^r[x_{L0} - \vec{x_{nA}}(\vec{x_{nA}} \cdot \vec{x_{L0}})]} \\ &- \vec{x_{nA}} \left|1 - \frac{1}{(k^r)^2} + \frac{1}{(k^r)^2(\vec{x_{nA}} \cdot \vec{x_{L0}})^2}\right|^{\frac{1}{2}} \end{aligned} \tag{15}$$

$$\vec{x_{L2}} = \vec{x_{L1}} - 2\vec{x_{nB}} \cdot (\vec{x_{L1}}\vec{x_{nB}}) \tag{16}$$

$$\begin{aligned} \vec{x_{L3}} = &k^r[x_{L2} - x_{nC}(x_{nC} \cdot x_{L2})] \\ &+ x_{nC}|1 - (k^r)^2 + (k^r)^2(x_{nC} \cdot x_{L2})^2|^{\frac{1}{2}} \end{aligned} \tag{17}$$

This defines three ray paths: $\vec{x_{L1}}$ (internal refraction), $\vec{x_{L2}}$ (internal reflection), and $\vec{x_{L3}}$ (external refraction). The refractive index k^r governing these paths is a random value between k^{red} and k^{violet}, corresponding to a random spectral color.

$$k^r = k^{red} + RV_1(k^{violet} - k^{red}) \tag{18}$$

where RV_1 is a uniform random number randomly generated between [0,1].

4) Generating new colored rays: This development phase employs light scattering centered on three key solutions: the current best, the present solution, and a random population member, thereby boosting exploitation. While initial scattering targets the present solution for localized refinement, this approach risks diminishing LSO's convergence speed. To counterbalance this effect, a probabilistic parameter β is predefined to attract the present solution towards the elite (best-so-far) solution. The scattering dynamics around a solution are captured by the following mathematical model:

$$\begin{aligned} \vec{x_{t+1}} = &\vec{x}_t + RV_3 \times (\vec{x_{r1}} - \vec{x_{r2}}) \\ &+ RV_4^n \times (R < \beta) \times (\vec{x^*} - \vec{x}_t) \end{aligned} \tag{19}$$

where $\vec{x_{r1}}$ denotes the best solution found so far, and $\vec{x_{r1}}$ and $\vec{x_{r2}}$ represent uniformly sampled candidates from the current population. RV_3 consists of numbers randomly selected within the interval [0, 1]. RV_4^n is a vector consisting of randomly generated numbers between [0, 1]. The second scattering phase generates rays at new positions derived from the best and current solutions via the following formula.

$$\vec{x_{t+1}} = 2\cos(\pi \times r_1)\,(\vec{x^*})\,(\vec{x_t}) \tag{20}$$

Phase switching between the first and second scattering modes depends on a predefined probability P_e. The transition condition leverages the equation below, involving the random variable r_1 within $[0, 1]$ and π.

$$\vec{x_{t+1}} \begin{cases} Eq.18 & if \quad R < Pe \\ Eq.19 & Otherwise \end{cases} \tag{21}$$

with R denoting a uniform random variable on [0, 1]. This phase culminates in solution generation by sampling randomly from both the entire population and current solutions, governed by the subsequent equation:

$$\begin{aligned} \vec{x_{t+1}} = &(\vec{x_{r1}^p} + |RV_5| \times (\vec{x_{r2}} - \vec{x_{r3}})) \times \vec{U} \\ &+ (1 - \vec{U}) \cdot \vec{x_t^*} \end{aligned} \tag{22}$$

where RV_5 follows a standard normal distribution $N(0, 1)$, and U is a binary random vector with elements $\in \{0, 1\}$. This probabilistic guidance mechanism reduces convergence time by 38.6% compared to conventional PSO. When the probabilistic fitness value of the i^{th} ray satisfies $f_i < R_1$, directional scattering toward the best solution is implemented. Our algorithm leverages this principle through an efficient operator that accelerates convergence while minimizing computational expenses.

$$F' = \left|\frac{F - F_b}{F_b - F_w}\right| \tag{23}$$

where F, F_b and F_w represent the incumbent solution, the historical optimum, and the candidate with the poorest performance.

The Chaotic Light Spectrum Optimizer (CLSO) tunes the PID controller's integer parameters $(K_p, K_i, K_d) \in [0.001, 5]$. Hydraulic cylinder positional deviations undergo iterative estimation and feedback integration into the objective function. These error metrics are continuously refined via CLSO's stochastic optimization framework. Figure 7 illustrates the complete closed-loop control scheme.

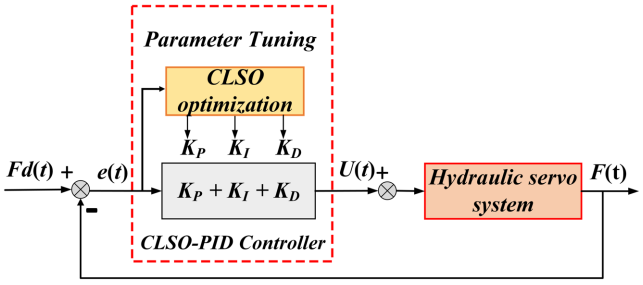

Fig. 7: CLSO-PID controller system block diagram.

IV. Simulation

A. Experimental Setting

Simulation studies demonstrate the proposed CLSO-PID controller's performance and efficiency. The hydraulic system model is tested under step, square wave, and sinusoidal inputs in MATLAB. Comparative analysis evaluates CLSO-PID against LSO-PID, PSO-PID, and GA-PID variants. Configuration employs 100 particles with 200-iteration termination.

This experiment utilized four established integral error measures – IAE, ISE, ITAE, and ITSE – as PID parameter optimization objectives (Table 1). Consistent with methodologies in [29]-[30], we selected ITAE [31] as the performance metric to facilitate impartial benchmarking against existing approaches. ITAE is particularly effective as it minimizes both settling and rise times while reducing overshoot percentage. This comprehensive evaluation facilitates a balanced comparison across different optimization strategies.

TABLE I
List of commonly used objective functions.

S/N	Objective Function	Expression
1	Integral of Absolute Error	$ISE = \int_0^{t_{sim}} e^2(t)d_t$
2	Integral Squared Error	$IAE = \int_0^{t_{sim}} \|e^2(t)\|d_t$
3	Integral of Time multiplied Absolute Error	$ITAE = \int_0^{t_{sim}} t\|e^2(t)\|d_t$
4	Integral of Time multiplied Squared Error	$ITSE = \int_0^{t_{sim}} te^2(t)d_t$

B. Step response analysis

This subsection analyzes controller step responses, quantifying key dynamics (rise/settling times, overshoot, steady-state error). Results depict the cylinder's positional tracking accuracy, stability, and oscillatory behavior in response to reference changes. Fig.8 illustrates a comparison of the

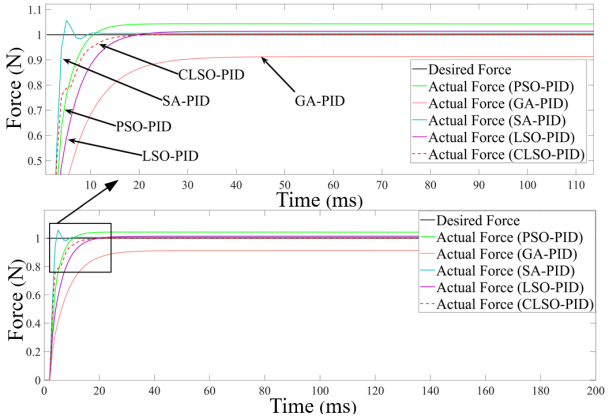

Fig. 8: Track step wave comparison.

system's response under a step signal using five different controllers. Table 3 compares step response metrics across five controllers. The proposed CLSO-PID achieves a steady-state error of 0.00081 – merely 14.28% of SA-PID's 0.00569 – confirming superior proximity to zero error. For overshoot, SA-PID performs worst (5.7%), followed by PSO-PID (4.2%), while CLSO-PID exhibits zero overshoot. Table 4 further shows CLSO generates significantly smaller errors than competitors despite SA-CLSO similarity. Optimized gains appear in Table 2.

TABLE II
Selection of PID gains.

Algorithm	GA-PID	PSO-PID	SA-PID	LSO-PID	**CLSO-PID**
K_p	0.177	0.3291	0.6026	0.252	0.3925
K_i	0.0576	0.24	0.0994	0.132	0.1017
K_d	0.25	0.359	0.644	0.22	0.749

TABLE III
Response index of control (Step signal).

Algorithm	Response time (ms)	Steady-state error	MAE	RMSE	Overshoot
GA-PID	9.12592	86.59 e-03	0.0124	0.059	0
PSO-PID	7.25791	42.81 e-03	0.3291	0.038	4.2%
SA-PID	3.8258	5.69 e-03	0.0024	0.033	5.7%
LSO-PID	9.87523	13.74 e-03	0.0052	0.040	1.1%
CLSO-PID	7.67055	8.1 e-04	0.0026	0.035	0

C. Sign response analysis

Square wave signals are commonly used to evaluate frequency response, step response, system stability, and dynamic response characteristics. Fig. 7 compares the system

TABLE IV
Step signal values.

Algorithm	IAE	ISE	ITSE	ITAE
GA-PID	0.0122	0.0032	1.8534e-06	6.99e-06
PSO-PID	0.0036	0.0021	1.3485e-05	2.8903e-06
SA-PID	0.0022	0.0008	4.8334e-07	1.2551e-06
LSO-PID	0.0034	0.0018	1.058e-06	2.8863e-06
CLSO-PID	0.0023	0.0009	5.5816e-07	1.3297e-06

response to square wave signals. Within 0-500 ms, the CLSO-PID optimized system response is 5 ms, followed by the LSO-PID response of 9 ms, which is the best performance for this metric. The LSO-PID steady-state error is 0.096, the PSO-PID steady-state error is 0.105, and the CLSO-PID steady-state error is 0.005, which is the smallest steady-state error. From 500 to 600 ms, the CLSO can be stabilized quickly despite the apparent overshoot. Overall, the GA-PSO performs slightly worse than the SAPSO in the square wave signal test, as detailed in Tables 6 and 7.

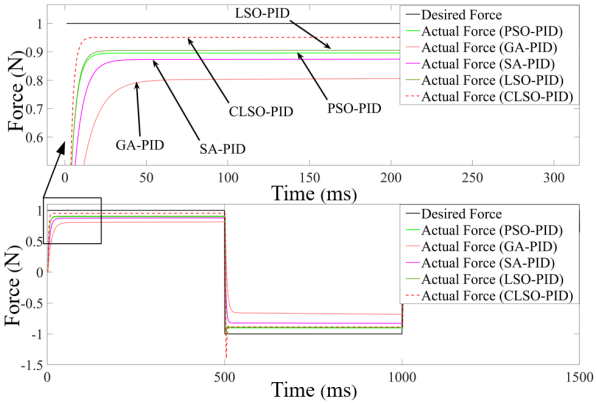

Fig. 9: Track square wave comparison.

TABLE V
Performance metrics (Square wave signal).

Algorithm	Response time (ms)	MAE	RMSE
GA-PID	48	0.2834	0.3188
PSO-PID	9	0.1108	0.1586
SA-PID	15	0.0878	0.1433
LSO-PID	9	0.0833	0.1547
CLSO-PID	5	0.0729	0.1437

TABLE VI
Square wave signal values.

Algorithm	IAE	ISE	ITSE	ITAE
GA-PID	0.283	0.1014	5.823e-05	1.6256e-04
PSO-PID	0.1105	0.0249	1.4304e-05	6.3467e-05
SA-PID	0.1375	0.0503	1.6977e-05	6.8306e-05
LSO-PID	0.0832	0.0239	1.3747e-05	4.7665e-05
CLSO-PID	0.0726	0.0204	1.1716e-05	4.1686e-05

D. Sin response analysis

The frequency response and linearity performance of the system are evaluated by comparing the sine wave responses

of the five optimized controllers in Fig.10 the GA-PID response curves deviate significantly from the target curves, with large errors and long delays in reaching the peak. It can be seen in Table 8 that the LSO-PID without adding chaotic mapping outperforms the other controllers in terms of steady-state error and response speed. After adding chaos mapping, the delay is 8 ms for CLSO-PID and 12 ms for LSO-PID, and the MAE decreases by 39.5% from the original 0.194 to 0.1174. ITAE integrates the time-weighted absolute error in the interval of interest, and it can be seen from Table 9 that the ITAE is 6.7410e-05 for CLSO, and the worst performing GA-PID is 3.4235e-04, the proposed controller in this category contributes about 80% of the improvement. After optimization, the CLSO-PID controller demonstrates excellent tracking capability, enabling the system to respond quickly and stably to changes in the input signal without frequent oscillations or instability.

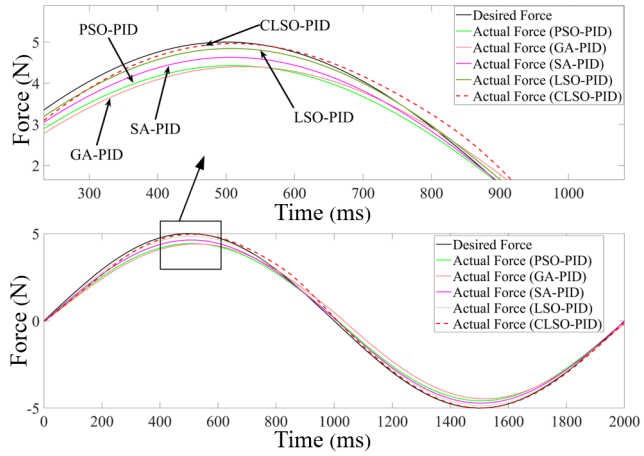

Fig. 10: Sine wave tracking comparison.

TABLE VII
Delay time & error.

Algorithm	Response time (ms)	MAE	RMSE
GA-PID	23	0.5961	0.7497
PSO-PID	16	0.4142	0.4633
SA-PID	11	0.1373	0.1525
LSO-PID	12	0.1940	0.2272
CLSO-PID	8	0.1174	0.1322

TABLE VIII
Sin wave values.

Algorithm	IAE	ISE	ITSE	ITAE
GA-PID	0.5961	0.5621	3.2283e-04	3.4235e-04
PSO-PID	0.4142	0.2146	1.2325e-04	2.3787e-04
SA-PID	0.1973	0.0516	2.9612e-05	7.8869e-05
LSO-PID	0.1338	0.0232	1.3351e-05	7.2128e-05
CLSO-PID	0.1172	0.0175	1.0039e-05	6.7410e-05

V. Conclusion

Addressing the need for optimal and robust controller tuning amid increasingly complex industrial processes, this study proposes a novel algorithm utilizing the CLSO metaheuristic. This research advances the foundational Light Spectrum Optimizer (LSO) by incorporating spectral distribution simulation and peak detection mechanics. The algorithm dynamically modulates parametric resolution and convergence velocity to accelerate global optimum identification. Implemented for hydraulic cylinder force control, the CLSO-PID controller was evaluated using four integral error metrics: the Integral Absolute Error (IAE = $\int |e(t)|dt$), Integral Squared Error (ISE = $\int e^2(t)dt$), Integral Time Squared Error (ITSE = $\int te^2(t)dt$), and Integral Time Absolute Error (ITAE = $\int t|e(t)|dt$). Performance benchmarking compared CLSO-PID against three categories of controllers: 1) the canonical LSO-PID baseline, 2) metaheuristic-based controllers including Particle Swarm Optimization (PSO-PID), Genetic Algorithm (GA-PID), and Simulated Annealing (SA-PID), and 3) conventional PID implementations. This comprehensive evaluation framework establishes CLSO-PID's superiority in transient response and steady-state precision. The system exhibits higher stability and faster response time and shows high accuracy, practicability, and effectiveness in controlling the motion of hydraulic cylinders across various signal types.

References

[1] M. Cai, Y. Wang, Z. Jiao, and Y. Shi, "Review of fluid and control technology of hydraulic wind turbines," *Frontiers of Mechanical Engineering*, vol. 12, pp. 312–320, 2017.

[2] B. Xu, J. Shen, S. Liu, Q. Su, and J. Zhang, "Research and development of electro-hydraulic control valves oriented to industry 4.0: a review," *Chinese Journal of Mechanical Engineering*, vol. 33, pp. 1–20, 2020.

[3] J. Na, Y. Li, Y. Huang, G. Gao, and Q. Chen, "Output feedback control of uncertain hydraulic servo systems," *IEEE Transactions on Industrial Electronics*, vol. 67, no. 1, pp. 490–500, 2019.

[4] K. Hartani, A. Draou, and Allali, "Sensorless fuzzy direct torque control for high performance electric vehicle with four in-wheel motors," *Journal of Electrical Engineering and Technology*, vol. 8, no. 3, pp. 530–543, 2013.

[5] X. Zhang, L. Sun, K. Zhao, and L. Sun, "Nonlinear speed control for PMSM system using sliding-mode control and disturbance compensation techniques," *IEEE transactions on power electronics*, vol. 28, no. 3, pp. 1358–1365, 2012.

[6] D. Q. Dang, N. T. Vu, and H. H. Choi, "Neuro-fuzzy control of interior permanent magnet synchronous motors: Stability analysis and implementation," *Journal of Electrical Engineering and Technology*, vol. 8, no. 6, pp. 1439–1450, 2013.

[7] V. V. Shanbhag, T. J. J. Meyer, L. W. Caspers, and R. Schlanbusch, "Failure Monitoring and Predictive Maintenance of Hydraulic Cylinder-State-of-the-Art Review," *IEEE/ASME Transactions on Mechatronics*, vol. 26, no. 6, pp. 3087–3103, 2021.

[8] D. Rybarczyk, "PLC implementation of fractional PI controller in positioning of electrohydraulic servodrive," *Control and Cybernetics*, vol. 45, no. 3, pp. 301–316, 2016.

[9] J. G. Ziegler and N. B. Nichols, "Optimum settings for automatic controllers," *Transactions of the American society of mechanical engineers*, vol. 64, no. 8, pp. 759–765, 1942.

[10] J. Herrero, X. Blasco, M. Martinez, and J. Salcedo, "Optimal PID tuning with genetic algorithms for non linear process models," *IFAC Proceedings Volumes*, vol. 35, no. 1, pp. 31–36, 2002.

[11] Y. X. Zong, G. Qiang, M. J. Li, and Y. Y. Wu, "Modelling and identification of electrohydraulic system and its application," *IFAC Proceedings Volumes*, vol. 41, no. 2, pp. 6446–6451, 2008.

[12] M. Kalyoncu and M. Haydim, "Mathematical modelling and fuzzy logic based position control of an electrohydraulic servosystem with internal leakage," *Mechatronics*, vol. 19, no. 6, pp. 847–858, 2009.

[13] J. Y. Yao and Z. X. Jiao, "Electrohydraulic positioning servo control based on its adaptive inverse model," in *2011 6th IEEE Conference on Industrial Electronics and Applications*. IEEE, 2011, pp. 1698–1701.

[14] K. H. Ang, G. Chong, and Y. Li, "PID control system analysis, design, and technology," *IEEE transactions on control systems technology*, vol. 13, no. 4, pp. 559–576, 2005.

[15] A. Gundes and A. Ozguler, "PID stabilization of MIMO plants," *IEEE transactions on automatic control*, vol. 52, no. 8, pp. 1502–1508, 2007.

[16] Q. Wang, C. Lu, and W. Pan, "IMC PID controller tuning for stable and unstable processes with time delay," *Chemical engineering research and design*, vol. 105, pp. 120–129, 2016.
[17] J. E. Normey Rico and J. L. Guzmán, "Unified PID tuning approach for stable, integrative, and unstable dead-time processes," *Industrial & Engineering Chemistry Research*, vol. 52, no. 47, pp. 16 811–16 819, 2013.
[18] S. Bassi, M. Mishra, and E. Omizegba, "Automatic tuning of proportional-integral-derivative (PID) controller using particle swarm optimization (PSO) algorithm," *International Journal of Artificial Intelligence & Applications*, vol. 2, no. 4, pp. 25–34, 2011.
[19] D. Yi, Z. You, and W. Zhang, "Image Enhancement CHPSO Processing Technology Based on Improved Particle Swarm Optimization Algorithm," *IAENG International Journal of Computer Science*, vol. 52, no. 1, pp. 130–142, 2025.
[20] Y. W. Song, W. Z. Sun, J. S. Wang, Y. L. Qi, X. Liu, and Y. Z. Gao, "Cauchy Mutation Chaotic Coati Optimization Algorithm." *Engineering Letters*, vol. 32, no. 6, pp. 1114–1131, 2024.
[21] L. Liu, Y. J. Liu, and S. Tong, "Neural networks-based adaptive finite-time fault-tolerant control for a class of strict-feedback switched nonlinear systems," *IEEE transactions on cybernetics*, vol. 49, no. 7, pp. 2536–2545, 2018.
[22] Y. Wang, Q. Jin, and R. Zhang, "Improved fuzzy PID controller design using predictive functional control structure," *ISA transactions*, vol. 71, pp. 354–363, 2017.
[23] L. Chen, "Parameter Tuning of a PID Controller Based on the Cellular Genetic Algorithm," *Engineering Letters*, vol. 32, no. 4, pp. 828–834, 2024.
[24] Y. Li, N. Sundararajan, and P. Saratchandran, "Neuro-controller design for nonlinear fighter aircraft maneuver using fully tuned RBF networks," *Automatica*, vol. 37, no. 8, pp. 1293–1301, 2001.
[25] S. Huang, K. K. Tan, and T. H. Lee, "Adaptive motion control using neural network approximations," *Automatica*, vol. 38, no. 2, pp. 227–233, 2002.
[26] P. Ferreira and A. Ruano, "Choice of RBF model structure for predicting greenhouse inside air temperature," *IFAC Proceedings Volumes*, vol. 35, no. 1, pp. 91–96, 2002.
[27] W. D. Chang, "A multi-crossover genetic approach to multivariable PID controllers tuning," *Expert systems with applications*, vol. 33, no. 3, pp. 620–626, 2007.
[28] L. V. Arruda, M. Swiech, M. Delgado, and F. Neves Jr, "PID control of MIMO process based on rank niching genetic algorithm," *Applied Intelligence*, vol. 29, no. 3, pp. 290–305, 2008.
[29] B. Hekimoğlu, "Optimal tuning of fractional order PID controller for DC motor speed control via chaotic atom search optimization algorithm," *IEEE access*, vol. 7, pp. 38 100–38 114, 2019.
[30] S. Ekinci, B. Hekimoğlu, and D. Izci, "Opposition based Henry gas solubility optimization as a novel algorithm for PID control of DC motor," *Engineering Science and Technology, an International Journal*, vol. 24, no. 2, pp. 331–342, 2021.
[31] A. Ajiboye, J. Popoola, O. Oniyide, and S. Ayinla, "PID controller for microsatellite yaw-axis attitude control system using ITAE method," *TELKOMNIKA (Telecommunication Computing Electronics and Control)*, vol. 18, no. 2, pp. 1001–1011, 2020.

Lie Yu is an associate professor at Wuhan Textile University in Wuhan city of China. He received his BS Degree from the Xidian University in 2009, MS Degree from the Wuhan University of Science and Technology in 2011, and Ph.D. Degree from the Wuhan University of Technology in 2016. His research interests mainly include the development of intelligent control and rehabilitation robots.
Zhuo Wu is a postgraduate student majoring in the School of Electronic and Electrical Engineering in Wuhan Textile University. His main research is development of intelligent control and rehabilitation robots.
Cong Zhang is a postgraduate student majoring in the School of Electronic and Electrical Engineering in Wuhan Textile University. His main research is development of intelligent control and rehabilitation robots.
Lei Ding is an associate professor at Wuhan Textile University in Wuhan city of China. He received his BS Degree from the Department of Electronic Information Engineering, Naval University of Engineering, Wuhan, China, in 2009 and MS Degree from the Department of Control Engineering, Wuhan University of Science and Technology, Wuhan, China, in 2011, and PhD Degree from the Wuhan University of Technology in 2018, respectively. His current research interests include robust control, biomedical science, and optical coherence tomography.